Path-length distribution of photoelectrons emitted from homogeneous noncrystalline solids: Consequences for inelastic-background analysis

I. S. Tilinin and A. Jablonski
Institute of Physical Chemistry, Polish Academy of Sciences, ulica Kasprzaka 44/52, 01-224 Warsaw, Poland

S. Tougaard
Institute of Physics, Odense University, Campusvej 55, DK-5230 Odense M, Denmark
(Received 23 January 1995)

The path-length distribution function characterizing the probability for a photoelectron to escape from a homogeneous solid after traveling a certain path length R has been found analytically by solving a Boltzmann-type kinetic equation with appropriate boundary condition. The solution is obtained in the transport approximation and is valid for an arbitrary geometry and under the condition that the typical angular spectrum of photoelectrons is a smooth function of the angular variable. It is shown that, depending on the initial anisotropy of the photoelectron emission, the path-length distribution may either reach a maximum value at a certain path length or be a monotonically decreasing function. The path-length distribution has also been calculated by the Monte Carlo technique employing realistic Mott differential elastic-scattering cross sections. The theoretical results were obtained for a number of photoelectron lines in Al, Cu, and Au with different asymmetry parameters and photoelectron energies. It was shown that within about 10% accuracy the path-length distribution function is a universal function of the path length divided by the transport mean free path. This conclusion is in full accordance with the prediction of the transport approximation. The consequences and implications of elastic-scattering effects for the inelastic background analysis of Auger electron spectroscopy and x-ray photoemission spectroscopy energy spectra are discussed.

I. INTRODUCTION

The energy spectra of photon-excited core electrons emitted from solids are influenced by the inelastic-scattering processes experienced by the electrons on their way out of the solid. The electron energy loss depends on the path-length distribution function $Q(R,\Omega)$ which describes the probability for a photoelectron generated inside a sample to leave the surface in the direction Ω after traveling the path length R (here Ω is a unit vector along the particle velocity). Knowledge of $Q(R,\Omega)$ for Auger electrons or photoelectrons makes it possible to evaluate the energy spectrum of the peak, provided that the inelastic-scattering cross section for electrons moving in the sample is known.[1] The geometrical configuration corresponding to a typical x-ray photoemission (XPS) experiment is shown schematically in Fig. 1. A target is irradiated by a beam of x rays incident at the polar angle θ. Photoelectrons generated inside the sample and leaving the surface, in a given direction, without a major energy loss are collected by the analyzer. The monitored energy spectrum of signal electrons in the vicinity of the characteristic peak is proportional to a convolution of the path-length distribution function and the energy distribution as a function of the traveled path length.[2] The path-length distribution function is therefore important for a quantitative interpretation of electron energy spectra, and has been the subject of several investigations in the past.[1-8]

Different analytical models have been applied to determine the path-length distribution. The most general theoretical approach is based on solving a kinetic Boltzmann equation (Ref. 9, p. 6). Although the exact solution of the kinetic equation may be obtained by Case's method of singular eigenfunctions (Ref. 9, p. 87), this procedure is rather complex in practical applications.[10] For this reason, several approximate solutions were attempted in the past. The quantity $Q(R,\Omega)$ was calculated analytically in the diffusion approximation by Tougaard and Sigmund.[2] Later, the P_1 approximation approach was applied by Tofterup[3] and Dwyer and Matthew[5] to describe the energy spectrum in the vicinity

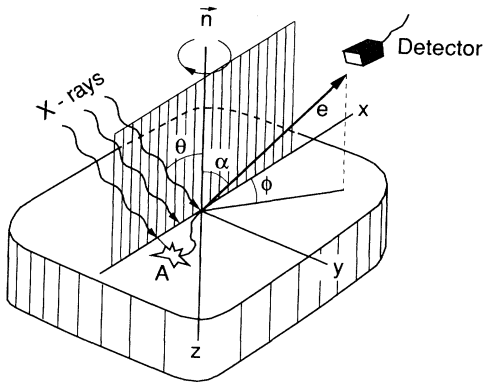

FIG. 1. Outline of the XPS configuration and the notation used.

of the characteristic peak.

Whereas the diffusion approximation becomes valid for large path lengths, it is inadequate to describe the function $Q(R,\Omega)$ for electrons in the vicinity of the peak, where the typical electron has traveled a path length only of the order of a few inelastic mean free paths. In addition, the latter approximation implies an expansion of the distribution function into a sum containing only the first two Legendre polynomials, which obviously do not form the complete set of solutions of the transport equation. As a result, the boundary condition at the target surface cannot be satisfied.

A relatively new development in the field of approximate solutions of the kinetic equation is the so-called transport approximation.[7,11–13] Within this approximation, the actual elastic-scattering cross section is replaced by the uniform cross section, equal to the corresponding momentum-transfer cross section. This makes possible an analytical solution of the resulting integrodifferential equation for a number of problems associated with electron transport. The transport approximation was successfully applied to determine the emission depth distribution function,[11,12] photoelectron intensity for different XPS configurations,[7,12] and the elastic backscattering probability of electrons from solids.[13]

The path-length distribution function can also be calculated using the Monte Carlo approach. In the published algorithms,[14,15] the generated path lengths were directly used for calculating the photoelectron intensity. However, with a slight modification, the same algorithm can be used to estimate the path-length distribution.

In the present work, we consider different theoretical models to evaluate the function $Q(R,\Omega)$. This function is derived analytically within the transport approximation and by the Monte Carlo technique. Using the calculated functions $Q(R,\Omega)$, we also investigate the influence of elastic photoelectron scattering on the shape of the XPS spectra and the inelastic background intensity.

II. THEORY

A. Common formalism of XPS

Elastic scattering of photoelectrons is neglected in the formalism routinely used in a quantitative XPS analysis. Let us consider a layer of thickness dz at a depth z. The contribution to the recorded signal strength, dY, corresponding to the considered layer, is given by the following expression:[16]

$$dY = TDF_x(A_0/\cos\alpha)\Delta\Omega M(d\sigma_x/d\Omega) \times \exp[-z/(\lambda_i\cos\alpha)]dz \ , \quad (1)$$

where T is the analyzer transmission function, D is the detector efficiency, F_x is the flux of incident x rays, A_0 is the analyzed area at the normal direction of analysis, $\Delta\Omega$ is the solid acceptance angle of the analyzer, M is the atomic density of the element, λ_i is the inelastic mean free path of the analyzed photoelectrons, and α is the detection angle with respect to the surface normal. In Eq. (1), $d\sigma_x/d\Omega$ denotes the differential photoelectric cross section. For unpolarized radiation and a random orientation of atoms or molecules, this cross section is given by[17]

$$d\sigma_x/d\Omega = \sigma_x\frac{1}{4\pi}\left[1-\frac{\beta}{4}(3\cos^2\Theta-1)\right]=\sigma_x S(\Omega) \ , \quad (2)$$

where σ_x is the total photoelectric cross section, Θ is the angle between the direction of x rays and the direction of the analysis, and β is the so-called asymmetry parameter. We see from Eq. (1) that, in this formalism, the photoelectron trajectory lengths corresponding to the considered layer are assumed to be identical and equal to $z/\cos\alpha$.

In the typical experimental XPS arrangement, a semi-infinite solid is exposed to a broad beam of x rays, irradiating an area much larger than the area being analyzed. Usually it is assumed that the analyzed area is proportional to $1/\cos\alpha$, and this accounts for the corresponding term in Eq. (1).

Within the common XPS formalism, the photoelectron creation is assumed to be uniform in the layer submitted to analysis. This assumption is reasonable in view of the much stronger attenuation of photoelectrons than that of x rays in the solid. Consequently, the flux F_x is independent of the depth z.

Assuming a homogeneous-in-depth composition of the solid, after integration of Eq. (1) over all depths we obtain

$$Y = C\lambda_i\mu S(\Omega) \ , \quad (3)$$

where

$$C = TDF_x(A_0/\mu)\Delta\Omega M\sigma_x \ , \quad (4)$$

and $\mu=\cos\alpha$. Ebel *et al.*[18] have shown that deviations from the above model of photoelectron transport result in a distribution of the length of trajectories originating from a given layer. They indicated that this may be due to (i) a large solid acceptance angle of the analyzer, (ii) surface roughness, and (iii) elastic photoelectron collisions. Knowledge of this distribution leads to a more realistic formalism describing the photoelectron intensity. In the present work, we approach the problem of the trajectory length distribution assuming a small solid angle of the analyzer. In experimental practice of XPS, indeed, the acceptance angles usually vary within a few degrees (e.g., 1.4° or 4.1°; cf. Ref. 14). Let us denote by $q(R,\Omega,z)$ the distribution of the lengths R of trajectories originating at a depth z. Equation (1) can be written as

$$dY = \frac{C\mu}{4\pi}\int_0^\infty q(R,\Omega,z)\exp(-R/\lambda_i)dR\,dz, \quad z<R<\infty \ , \quad (5)$$

where

$$q(R,\Omega,z) = 4\pi S(\Omega)\delta(\mu R - z) \ , \quad (6)$$

and $\delta(x)$ is the Dirac function. The integration with respect to the depth, z, can be performed as follows:

$$Y = \frac{C\mu}{4\pi}\int_0^\infty Q(R,\Omega)\exp(-R/\lambda_i)dR \ , \quad (7)$$

where $Q(R,\Omega)$ is the total path-length distribution

$$Q(R,\Omega)=\int_0^\infty q(R,\Omega,z)dz \ . \tag{8}$$

For the common XPS formalism, from Eqs. (6) and (8) we have

$$Q(R,\Omega)=4\pi S(\Omega)=\text{const} \ . \tag{9}$$

It follows from Eqs. (2) and (9) that, within the considered formalism, the path-length distribution is only a function of the XPS configuration. However, due to elastic photoelectron collisions, the function $q(R,\Omega,z)$ depends on the path length R in a much more complicated way than that described by expression (6), and, consequently, function $Q(R,\Omega)$ is no longer a constant. Since the knowledge of the path-length distribution is of crucial importance for a quantitative XPS analysis [cf. Eq. (7)], in the present work, the function $Q(R,\Omega)$ was determined from the Monte Carlo algorithm and from the transport approximation. Details of both theoretical approaches are given in the following sections.

B. Transport approximation

Let us consider the XPS configuration shown in Fig. 1. The electrons generated inside the target by photoionization of atoms escape from the sample in the direction Ω specified by the polar angle α counted from the surface normal and the azimuthal angle ϕ counted from the plane of incidence. The initial angular distribution of photoelectrons emitted in the sample, $S(\Omega)$, is assumed to be described by the probability density function given by Eq. (2), in which Θ is now the angle between vector Ω and the direction of x rays. We denote by $Y(\Omega)d\Omega$ the differential yield of photoelectrons escaping from the sample in the direction $(\Omega,d\Omega)$ without being scattered inelastically. Furthermore, let us denote by $N(z,R,\Omega)$ the flux density of electrons moving at the depth z in the direction Ω after traveling the path length R. The trajectory length distribution function is related to the flux density by the equation

$$Q(R,\Omega)=4\pi N(z=0,R,\Omega) \ . \tag{10}$$

Hence to find the path-length distribution function one should determine the electron flux density N. The latter quantity satisfies the kinetic equation with the boundary condition implying that no secondaries enter the sample. Thus, applying the transport approximation, we have

$$\nu\frac{\partial N}{\partial\tau}=-N+(4\pi)^{-1}\int_{4\pi}d\Omega'(\tau,\Omega'\rho)-\frac{\partial N}{\partial\rho}+S(\Omega)\delta(\rho) \ , \tag{11}$$

$$N(\tau=0,\Omega,\rho)=0 \quad \text{for } \nu>0 \ , \tag{12}$$

where ν is the cosine of the polar angle between vector Ω and the z axis, τ is the dimensionless depth

$$\tau=z/\lambda_{\text{tr}} \ ,$$

ρ is the dimensionless path length

$$\rho=R/\lambda_{\text{tr}} \ ,$$

and λ_{tr} denotes the so-called transport mean free path defined by

$$\lambda_{\text{tr}}=\left[2\pi M\int_0^\pi(1-\cos\xi)\frac{d\sigma}{d\Omega}\sin\xi d\xi\right]^{-1} \ ,$$

where $d\sigma/d\Omega$ is the differential elastic-scattering cross section, and ξ is the polar scattering angle. Note that negative values of $\nu<0$ correspond to electrons moving toward the surface, while positive ν values refer to electrons moving toward the bulk of the target. Equation (11) follows from the usual time-dependent transport equation for a nonabsorbing medium (Ref. 9, p. 16) when taking into account that the path length traveled by the electron is related to the time t and the particle velocity v by the simple formula $R=vt$.

We are looking for a solution of the problem, defined by Eqs. (11) and (12), in the form

$$N(\tau,\Omega,\rho)=(2\pi i)^{-1}\times\int_{4\pi}d\Omega_0 S(\Omega_0)\times\int_{\gamma-i\infty}^{\gamma+i\infty}G_p(\tau,\Omega|\Omega_0)\exp(p\rho)dp \ , \tag{13}$$

where γ is located to the right of the integrand singularities (Ref. 9, p. 175), and the Green's function $G(\tau,\Omega,\Omega_0)$ satisfies the equation

$$\nu\frac{\partial G_p}{\partial\tau}=-\zeta(p)^{-1}G_p+(4\pi)^{-1}\int_{4\pi}G_p(\tau,\Omega'|\Omega_0)d\Omega'+\delta(\Omega-\Omega_0) \ , \tag{14}$$

with a boundary condition of type (12). In Eq. (14), the single scattering albedo, $\zeta(p)$, reads

$$\zeta(p)=(1+p)^{-1} \ . \tag{15}$$

The solution of Eq. (14) with the boundary condition of type (12) can be found by splitting the Green's function into two components.[19] The first component corresponds to the solution of the secondary emission problem for an isotropic source of power, $\zeta/4\pi$, while the other is proportional to the Green's function for the albedo problem in the case of an isotropically scattering medium.[20] More details are available elsewhere.[19] In particular, the value of the Green's function G_p at the surface for $\nu<0$ is given by the expression

$$G_p(0,\Omega|\Omega_0)=T_p(\Omega,\Omega_0) \quad \text{for any } \nu<0 \ , \tag{16}$$

where

$$T_p(\Omega,\Omega_0)=\frac{\zeta(p)H[-\nu,\zeta(p)]}{4\pi[1-\zeta(p)]^{1/2}}+\begin{cases}-\dfrac{\zeta(p)\nu_0 H[-\nu,\zeta(p)]H[\nu_0,\zeta(p)]}{4\pi(\nu_0-\nu)} & \text{for } \nu_0>0\\ \delta(\Omega-\Omega_0) & \text{for } \nu_0<0.\end{cases} \tag{17}$$

In the latter expression $H(\nu,\zeta)$ is the H function of Chandrasekhar.[20]

Substitution of formula (16) into (13) yields the explicit expression for the outgoing flux density of photoelectrons $N(0,\Omega,\rho)$. Then, by making use of relationship (10), we arrive at the final result for the path-length distribution function:

$$Q(R,\Omega)=(2\pi i)^{-1}\int_\Gamma \zeta(p)\left\{[1-\zeta(p)]^{-1/2}H[\mu,\zeta(p)]-(\beta/4)[3\cos^2\Theta-1]\right.$$
$$\left.+[\beta(3\mu_\gamma^2-1)/16]\zeta(p)\int_0^1 xH[x,\zeta(p)]H[\mu,\zeta(p)](x+\mu)^{-1}(3x^2-1)dx\right\}\exp(p\rho)dp\ . \tag{18}$$

In formula (18) $\mu=\cos\alpha$, and μ_γ is the cosine of the incidence angle of x rays. The contour of integration Γ in Eq. (18) embraces the cut from -1 to 0 along the real axis in the complex p plane. In the case of an initially isotropic angular distribution ($\beta=0$), expression (11) reduces to formula (17) of Ref. 7.

To facilitate an analysis of the path-length distribution behavior, it is advisable to present the function $Q(R,\Omega)$ in terms of real integrals. For this purpose we rewrite Eq. (18) in the following way:

$$Q(R,\Omega)=K_1(\rho,\mu)-(\beta/4)[3\cos^2\Theta-1]\exp(-\rho)+[\beta(3\mu_\gamma^2-1)/16]K_2(\rho,\mu)\ , \tag{19}$$

where the notation

$$K_1(\rho,\mu)=(2\pi i)^{-1}\int_\Gamma \zeta(p)[1-\zeta(p)]^{-1/2}H[\mu,\zeta(p)]\exp(p\rho)dp\ , \tag{20}$$

$$K_2(\rho,\mu)=(2\pi i)^{-1}\int_\Gamma \zeta^2(p)\int_0^1 xH[x,\zeta(p)]H[\mu,\zeta(p)](x+\mu)^{-1}(3x^2-1)dx\exp(p\rho)dp \tag{21}$$

is introduced. Integrals (20) and (21) over the complex p variable can be reduced to real integrals along the upper and lower edges of the cut from -1 to 0. By applying the approximate expression for the H function of Chandrasekhar,[7]

$$H[\mu,\zeta]=H(\mu,1)\{1+[H(\mu,1)-1](1-\zeta)^{1/2}\}^{-1}\ , \tag{22}$$

the integrals mentioned above may be transformed to the expressions

$$K_1(\rho,\mu)=k\int_0^1[(1-u)/u]^{1/2}[1+uV(\mu)]^{-1}\exp(-u\rho)du\ , \tag{23}$$

$$K_2(\rho,\mu)=k\exp(-\rho)\int_0^1\left\{u^{1/2}(1-u)^{-1/2}\{\exp[\rho(1-u)]-1\}\int_0^1\frac{xH(x,1)(3x^2-1)[H(\mu,1)+H(x,1)-2]}{[1+uV(\mu)][1+uV(x)](x+\mu)}dx\right\}du\ . \tag{24}$$

The factors k and V in formulas (23) and (24) are defined by the equations

$$k^{-1}=\int_0^1[(1-u)/u]^{1/2}[1+uV(\mu)]^{-1}du\ ,$$
$$V(t)=[H(t,1)-1]^2-1\ . \tag{25}$$

The accuracy of the approximate formulas (23) and (24) is about 1–2%. Expression (19) together with Eqs. (23)–(25) is very convenient for numerical evaluation of the path-length distribution function. Close inspection of the terms entering the right-hand side of Eq. (19) reveals that the third term is usually small compared with the first two terms. The first term diminishes very slowly with increasing path length ρ, proportionally to $\rho^{-1/2}$ (cf. Ref. 7). From a physical point of view, it corresponds to the randomized fraction of the photoelectron flux since no dependence on the initial emission direction as well as on the angle of incidence of x rays is present. The second term may be either negative or positive depending on the angle Θ. This part of the path-length distribution function describes the influence of anisotropy of photoemission. In the transport approximation, information about the anisotropy is retained by particles that are not scattered at all or that experience multiple small-angle deflections. That is why the second term decays exponentially and the rate of decay is determined by the transport mean free path λ_{tr}. Due to this fact, an interesting competition occurs between the first and second terms. Consider, for example, the case of normal emission and incidence and the asymmetry parameter being equal to $\beta=2$. In this situation no photoelectrons are initially emitted in the direction $\mu=1$. As a result the path-length distribution function is zero for $\rho=0$ and $Q(0,\Omega)=0$. However, owing to elastic-scattering effects some electrons after traveling a certain path length may change their direction of motion and escape from the sur-

face along the normal. In this case, the function Q will have a maximum at the path length $\rho_0 \sim 1.5$.

C. Monte Carlo scheme

The Monte Carlo approach has frequently been used to describe photoelectron transport in solids.[14,15] These calculations were devoted to the problems of the angular distribution of photoelectron emission, photoelectron intensity, and the sampled depth. The algorithm used in the present work for calculations of the trajectory length distribution was based on assumptions similar to the algorithms published earlier. These assumptions are briefly summarized below.

(1) The scattering potential corresponding to the scattering centers of the solid is approximated by the Thomas-Fermi-Dirac potential. The total scattering cross section σ_t, and the differential elastic-scattering cross sections $d\sigma/d\Omega$, are determined for this potential prior to Monte Carlo calculations.

(2) The elastic-scattering events along the photoelectron trajectory are assumed to follow the Poisson stochastic process. In that case, the linear step lengths between elastic collisions follow the exponential distribution

$$F(\Lambda)=(1/\lambda_e)\exp(-\Lambda/\lambda_e) ,$$

where λ_e is the elastic mean free path:

$$\lambda_e=(M\sigma_t)^{-1} .$$

(3) The scattering event is described in the local coordinates (the z axis in the direction Ω) by the azimuthal scattering angle and the polar scattering angle ξ. A uniform distribution, in the range from 0° to 360°, is assumed for the azimuthal scattering angles. The polar scattering angles are described by the distribution

$$f(\xi)=\frac{1}{\sigma_t}\frac{d\sigma}{d\xi}=2\pi\frac{1}{\sigma_t}\frac{d\sigma}{d\Omega}\sin\xi .$$

(4) The probability density function for the initial distribution of photoelectron emission is described by Eq. (2).

(5) Photoelectron emission is assumed to be uniform with depth, corresponding to a homogeneous solid.

The photoelectron trajectory was followed until the photoelectron left the solid, or until its length was too large to make a significant contribution to the intensity. In the present work, the largest length considered was equal to $10\lambda_i$. As in earlier calculations,[15] the solid acceptance angle of the analyzer was defined by the half-cone angle 10°. The value of the function $Q(R)$ for the interval $R\pm\Delta R$ was estimated from

$$Q(R)=\frac{1}{n}\sum_{i=1}^{n}\Delta_i(R) . \tag{26}$$

Suppose that the ith photoelectron traveled the distance R_i in the solid. The quantity $\Delta_i(R)$ for this photoelectron was assigned the following values:

$$\Delta_i(R)=\begin{cases}1 & \text{if } R-\Delta R<R_i<R+\Delta R \\ & \text{and the photoelectron entered the solid angle } \Delta\Omega \\ 0 & \text{in all other cases.}\end{cases} \tag{27}$$

The histogram resolution ΔR was $0.1\lambda_i$. To obtain good statistics, 3×10^7 photoelectron trajectories were generated for each energy and XPS configuration. The confidence interval was followed for the total photoelectron intensity corresponding to a given function $Q(R)$. This interval decreased below 1% in all considered cases.

III. RESULTS

Calculations of the trajectory length distribution function were made for photoelectrons ejected in elemental aluminum, copper, and gold by Mg $K\alpha$ radiation. The kinetic energies considered correspond to Al $2s$ (1135 eV), Cu $2p_{3/2}$ (320 eV), Cu $3s$ (1130 eV), Au $4s$ (491 eV), and Au $4f_{7/2}$ (1169 eV). For each kinetic energy, three values of the asymmetry parameter β were assumed: $\beta=0$, 1, and 2. This was made in order to establish the influence of the initial anisotropy on the shape of the function $Q(R,\Omega)$. Two XPS configurations were considered in the present work.

(1) $\alpha=15°$, $\phi=0°$, and $\theta=20°$. This is the geometry of the spectrometer based on the VG CLAM 100 analyzer. For this geometry $\Theta=35°$, and we expect that the elastic photoelectron collisions increase the peak intensity.[15]

(2) $\alpha=45°$, $\phi=0°$, and $\theta=45°$. For this geometry $\Theta=90°$, and the elastic-scattering effect is expected to decrease the peak intensity.[15]

The function $Q(R,\Omega)$ was calculated for three theoretical models, described in Sec. II: (i) the common XPS formalism, also called the straight-line approximation (SLA) [Eq. (9)]; (ii) the transport approximation [Eqs. (19) and (23)–(25)]; and (iii) the Monte Carlo simulation [Eqs. (26) and (27)]. Results of calculations for copper and gold are shown in Figs. 2 and 3. One can see that, in all cases, the transport approximation and the Monte Carlo algorithm provide very similar path-length distribution functions. The function $Q(R,\Omega)$ calculated from the Monte Carlo scheme, implementing the actual distribution of scattering angles, should be identical to the function resulting from the accurate solution of the kinetic equation. For this reason, the Monte Carlo results may be considered as a reference for testing the reliability of the approximate solutions. Figures 2 and 3 prove that the transport approximation is a powerful tool for determining the functions $Q(R,\Omega)$, the more so as the corresponding algorithm is several orders of magnitude faster

than the Monte Carlo calculations.

As follows from Figs. 2 and 3, the elastic photoelectron collisions considerably influence the shape of the trajectory length distribution. The value of the function $Q(R,\Omega)$ at $R=0$ resulting from the straight-line approximation is always the same as the value obtained from theories accounting for elastic scattering. This result is obvious since the probability of elastic collision within a short trajectory is low, and the straight-line approximation is then valid. Pronounced deviations are observed, however, for larger trajectory lengths. The shape of the function $Q(R,\Omega)$ depends dramatically on the XPS configuration and on the asymmetry parameter. This function, calculated from theories accounting for elastic collisions, may be smaller or larger than the constant value predicted by the straight-line approximation. In some cases, an involved shape with a maximum has been obtained. The analysis of the shape of the function $Q(R,\Omega)$ is facilitated by the normalization defined by Eq. (7). As follows from Eqs. (19) and (23)–(25), the function $Q(R,\Omega)$ within the transport approximation depends on a dimensionless variable ρ. This means that, for a given experimental geometry, the path-length distribution as a function of ρ is of a universal character, and its shape is independent of the material and the photoelectron kinetic energy. To verify this prediction, extensive comparisons were made with the Monte Carlo results. The universal curves calculated from Eqs. (19) and (23)–(25) are compared with the results of Monte Carlo calculations in Figs. 4 and 5. One can see that the agreement is very good. Somewhat larger deviations are observed only for photoelectrons in aluminum for $\beta=2$ (Al $2s$) and for geometry $\alpha=15°$ and $\theta=20°$. Furthermore, the shape of the universal curve depends critically on the geometry of experiment and the anisotropy of photoemission. This shape is very well reproduced by the Monte Carlo simulations over a wide range of energies and atomic numbers. Therefore, the universal curves calculated for the geometry of a given spectrometer and for several ranges of the asymmetry parameters make it possible to estimate the effects of elastic photoelectron collisions in quantitative XPS. An example of such an application is described below.

Evaluation of the model spectra

From the path-length distribution function $Q(R,\Omega)$, the photoelectron spectrum can be calculated from the expression[21]

$$J(E,\Omega)=\int dE_0 F(E_0)\int Q(R,\Omega)G(E_0,R;E)dR \ ,$$

where $F(E_0)$ is the primary excitation spectrum, and $G(E_0,R:E)$ is the distribution of electron energies E for an electron originally excited at energy E_0 as a function of path length R. The latter function is given by[22]

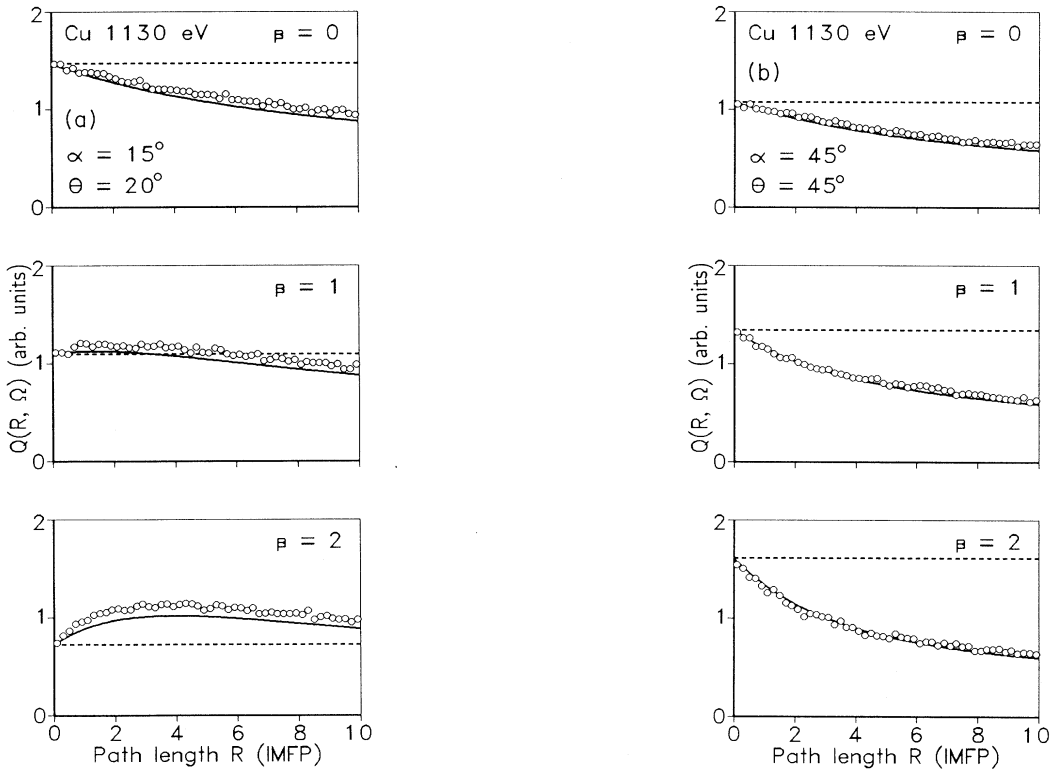

FIG. 2. The path-length distribution function calculated for 1130-eV electrons in elemental copper and for different values of the asymmetry parameter. Solid line: transport approximation; dashed line: straight-line approximation; circles: Monte Carlo calculations. (a) XPS configuration defined by $\theta=20°$ and $\alpha=15°$. (b) XPS configuration defined by $\theta=45°$ and $\alpha=45°$.

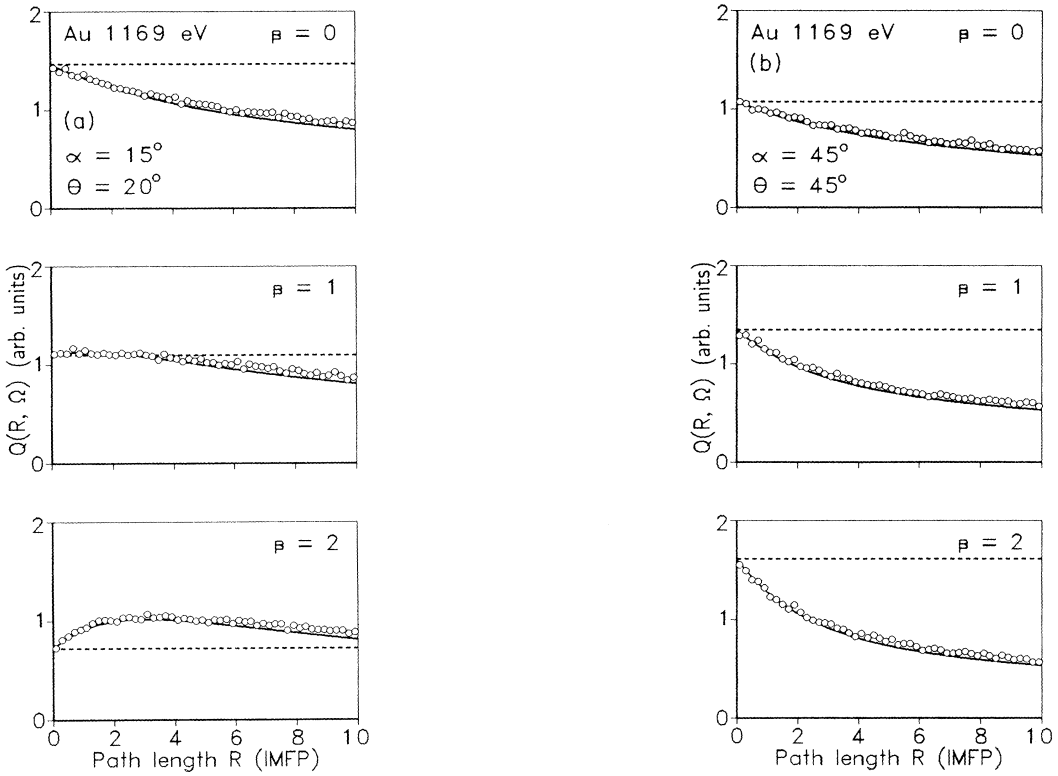

FIG. 3. The path-length distribution function calculated for 1169-eV electrons in elemental gold and for different values of the asymmetry parameter. Solid line: transport approximation; dashed line: straight-line approximation; circles: Monte Carlo calculations. (a) XPS configuration defined by $\theta=20°$ and $\alpha=15°$. (b) XPS configuration defined by $\theta=45°$ and $\alpha=45°$.

$$G(E_0,R;E)=1/(2\pi)\int ds\,\exp[is(E_0-E)-R\Sigma(s)]\ ,$$

where

$$\Sigma(s)=\int dT\,K(T)[1-\exp(-isT)]\ ,$$

and $K(T)$ is the inelastic electron-scattering cross section for energy loss T. In the present work this was done by applying an existing software package,[23] using the universal inelastic electron-scattering cross section.[24] The primary excitation spectrum $F(E)$ was taken to be an asymmetric Doniach-Sunjic line shape[25] with the width $\gamma=3$ eV and the asymmetry constant $\alpha=0.1$ centered at the respective peak energies. The results are shown in Figs. 6 and 7. The inelastic background, as well as the peak height, are distinctly affected by elastic photoelectron collisions. In the geometry defined by $\alpha=15°$ and $\theta=20°$, the spectrum intensity is increased or decreased depending on the anisotropy of the photoemission. These results are in agreement with recent studies of the influence of elastic scattering on the intensity of signal electrons emitted from gold.[15] The signal photoelectron intensity collected in the considered geometry has been found to be increased by elastic collisions for $0<\beta<2$.

The intensity of the photoelectron spectra calculated for the second geometry ($\alpha=45°$, $\theta=45°$) always decreases due to elastic collisions. Again, this result is in agreement with earlier studies.[15] The elastic-scattering effects, in this case, distinctly increase with increasing asymmetry parameter β.

In all cases considered, the peak shapes calculated using the $Q(R,\Omega)$ function obtained from the transport approximation and from Monte Carlo simulations are practically identical. One should note, however, that the time of computations associated with the transport approximation is shorter by several orders of magnitude as compared with the Monte Carlo approach. Both facts indicate a prospective use of the transport approximation for estimating the contribution of elastic-scattering effects in the inelastic background analysis.

On close analysis of Figs. 6 and 7, we see that the peak intensity and background are modified by elastic collisions in the same direction, i.e., either increased or decreased. A question arises if the intensity variation due to elastic collisions is equivalent to multiplication of the spectrum intensity by a certain constant factor. To check this hypothesis, we plotted the calculated spectra for Cu $3s$ photoelectrons ($\beta=2$) after normalization with respect to a common peak height (Fig. 8). We see that the background shape is still different for the SLA model and for models accounting for the elastic scattering. Thus a simple estimation of the contribution of elastic collisions to the spectra shape, by making use of a single correction factor, seems to be impossible.

IV. DISCUSSION

The exceptionally good performance of the transport approximation can be explained by applying the so-called

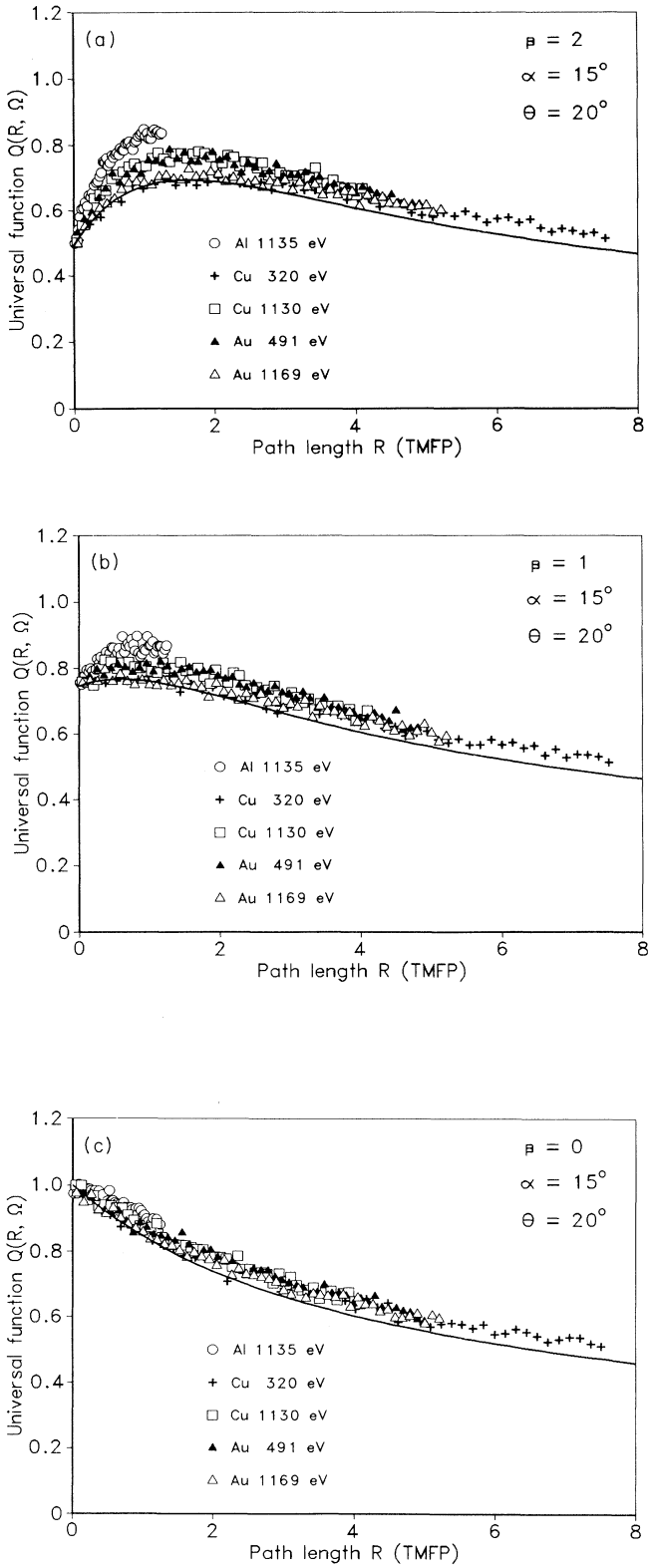

FIG. 4. Comparison of the universal path-length distribution function [Eqs. (19) and (22)–(25)] with results of the Monte Carlo calculations. The XPS configuration is defined by $\theta=20°$ and $\alpha=15°$. (a) $\beta=0$. (b) $\beta=1$. (c) $\beta=2$. Note that length is expressed in units of the transport mean free path.

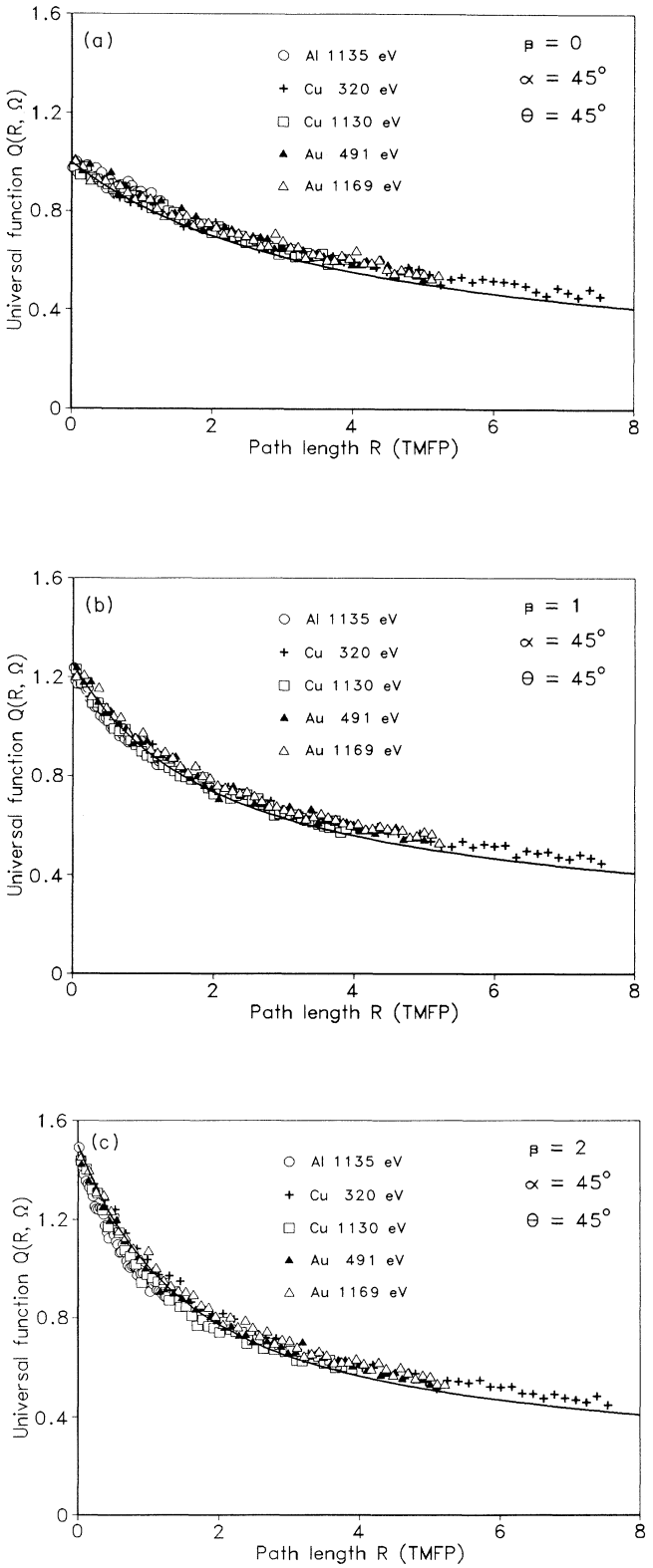

FIG. 5. Comparison of the universal path-length distribution function [Eqs. (19) and (22)–(25)] with results of the Monte Carlo calculations. The XPS configuration is defined by $\theta=45°$ and $\alpha=45°$. (a) $\beta=0$. (b) $\beta=1$. (c) $\beta=2$. Note that length is expressed in units of the transport mean free path.

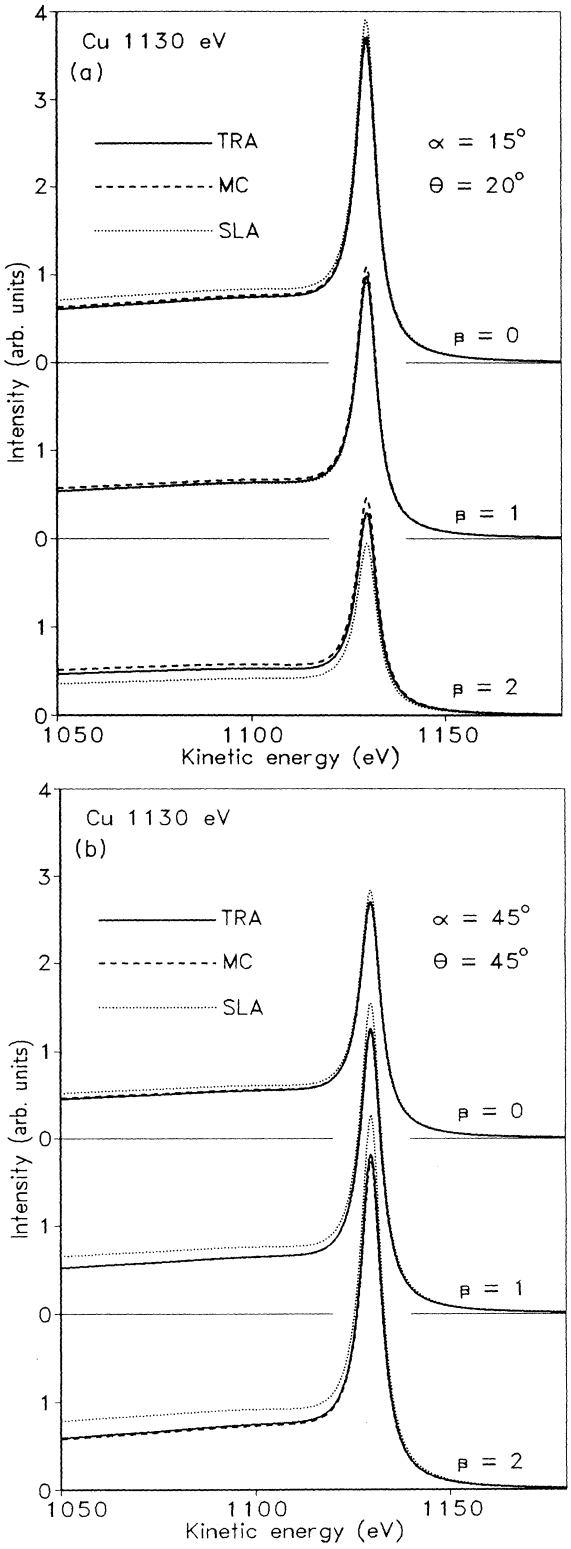

FIG. 6. The energy spectrum calculated from Eq. (28) for 1130-eV electrons in copper using the path-length distribution function resulting from different theoretical models. Solid line: transport approximation (TRA); dashed line: Monte Carlo calculations (MC); dotted line: straight-line approximation (SLA). (a) XPS configuration defined by $\theta=20°$ and $\alpha=15°$. (b) XPS configuration defined by $\theta=45°$ and $\alpha=45°$.

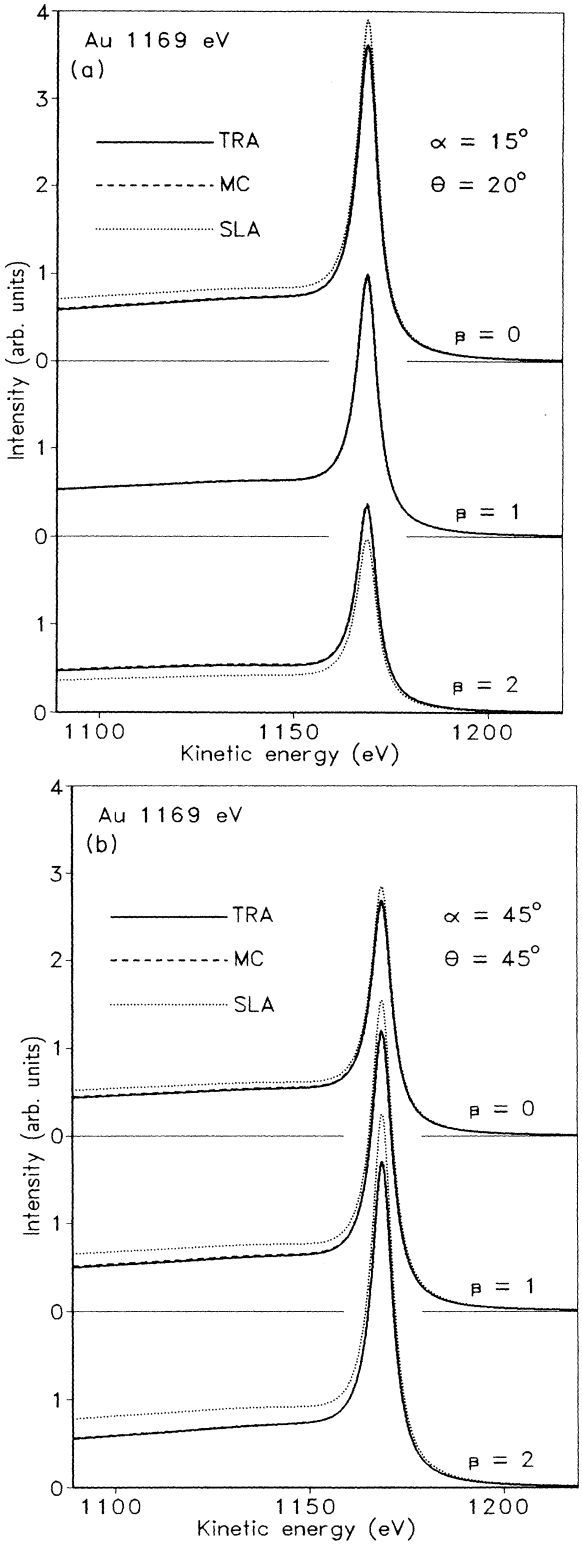

FIG. 7. The energy spectra calculated from Eq. (28) for 1169-eV electrons in gold using the path-length distribution function resulting from different theoretical models. Solid line: transport approximation (TRA); dashed line: Monte Carlo calculations (MC); dotted line: straight-line approximation (SLA). (a) XPS configuration defined by $\theta=20°$ and $\alpha=15°$. (b) XPS configuration defined by $\theta=45°$ and $\alpha=45°$.

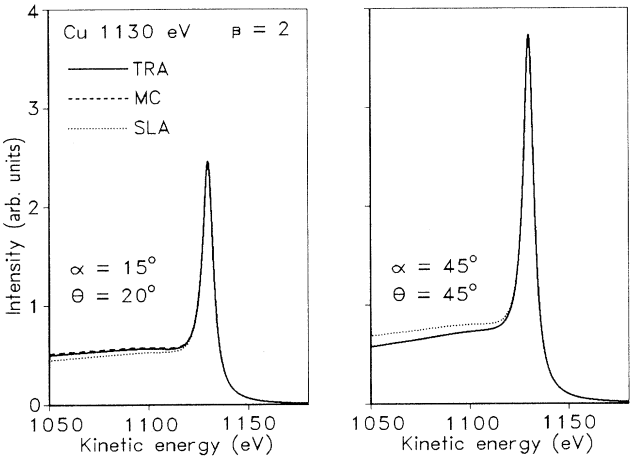

FIG. 8. The energy spectra calculated from Eq. (28) for 1130-eV electrons in copper using the path-length distribution function resulting from different theoretical models. Solid line: transport approximation (TRA); dashed line: Monte Carlo calculations (MC); dotted line: straight-line approximation (SLA). All spectra are normalized to a common height.

generalized radiative field similarity principle.[10,12] This principle may be considered as a criterion for reliability of any approximate solution of the kinetic equation.

According to the similarity principle, the exact differential elastic-scattering cross section may be replaced in the transport equation by an approximate cross section which makes possible an analytical solution of the boundary problem. However, this can be done only under the condition that the scattering cross section provides a similarity between exact and approximate solutions at least in the limiting cases of weak ($\lambda_i \gg \lambda_{tr}$) and strong ($\lambda_i \ll \lambda_{tr}$) absorption. Additionally, the initial angular distribution of electrons is assumed to be a smooth function of the angular variable, i.e., the following condition is satisfied:[11]

$$N \geq |\partial N/\partial \nu| \ .$$

The main postulate of the similarity principle is the statement that the approximate solution thus obtained is also close to the exact one in the intermediate case of scattering parameters ($\lambda_i \sim \lambda_{tr}$) when neither the straight line nor the diffusion approximations yield satisfactory results. The similarity of the exact and approximate radiative fields in the limiting cases mentioned above is achieved since (1) the approximate solution reduces to the straight-line approximation result when elastic scattering is negligible, and (2) the transport cross section is equal to the exact transport cross section. The latter requirement follows from the usual similarity relationship in the diffusion-limiting case.[26] This relationship has a simple physical meaning: the exact and approximate distribution decay rates at large distances from a source should be identical. The major corollary of the similarity relationship is that the particle transport is governed mainly by the momentum-transfer cross section in the limiting case of pronounced elastic scattering. Hence we arrive at the important conclusion that any approximate differential elastic-scattering cross section satisfying the similarity principle should be selected in such a way that it provides the same value for the transport cross section as the exact elastic cross section does. It should be emphasized that the generalized radiative similarity principle implies a much more powerful statement: the transport cross section governs the particle transport not only under the condition of pronounced elastic scattering but also in all other physical situations, provided the typical angular distribution is not highly anisotropic. Due to this fact, the transport mean free path gains much in importance in secondary-emission problems as one of the principal quantities of electron-solid interaction. The quasiclassical solution of the problem of elastic scattering in electron-atom collisions[27] allows one to evaluate analytically the momentum transfer cross section of medium-energy electrons and to study its dependence on the atomic number and the electron energy. It turns out that the ratio λ_i/λ_{tr} is of the order of unity in the energy range relevant for XPS.[10,28] Thus the generalized radiative field similarity principle may be an effective tool for solving photoelectron transport problems.

The path-length distribution $Q(R,\Omega)$ along with the depth distribution function[11,29] is one of the emission characteristics which are essentially length dependent. The remarkable feature of the path-length distribution is that it does not depend on the inelastic interaction quantities, in contrast to the escape probability. It follows from the above discussion that the only typical length of the radiative transfer process is the transport mean free path λ_{tr} when the absorption is negligible. Consequently, one can state without referring to a solution of the kinetic equation that the path-length distribution should be a function of the ratio R/λ_{tr} and a geometrical configuration if the generalized radiative field similarity principle is true. This conclusion is perfectly supported by comparison of the $Q(R,\Omega)$ function found in the transport approximation with the Monte Carlo calculations based on a realistic differential elastic-scattering cross section. The discrepancies between the universal dependence and the Monte Carlo data in the case of $\beta=2$ and the near-normal-incidence-emission geometry ($\alpha=15°$, $\theta=20°$) [Fig. 4(c)] are caused partially by the relatively large half-cone acceptance angle ($\Delta\alpha=\pm 10°$) used in the Monte Carlo simulation code. In the case of $\beta=2$, the path-length distribution function increases rapidly with increasing emission angle α for near-normal incidence of x rays. The Monte Carlo results represent the path-length distribution averaged over the solid angle defined by $\Delta\alpha$ and thereby slightly overestimate the value $Q(R,\Omega)$. The other reason for the discrepancies may be a higher degree of anisotropy of the angular distribution of photoelectrons escaping from atoms in near-normal directions. In the transport approximation, the actual shape of the exact differential elastic-scattering cross section is neglected. Therefore, specific features of elastic scattering of electrons which traveled the path lengths $R \ll \lambda_{tr}$ and thereby suffered 1–2 elastic collisions are not fully accounted for. Obviously, the influence of the

shape of the elastic cross section is more pronounced for higher anisotropy of the initial distribution and smaller ratios λ_e/λ_{tr} (here λ_e is the elastic mean free path). This may be especially significant in the case of aluminum, which is characterized by a sharply forward peaked differential elastic-scattering cross section.

The practical relevance of the analytical expression for the function $Q(R,\Omega)$ [formulas (18) and (19)] is prompted by its prospective application to the inelastic background substraction needed for the quantitative Auger electron spectroscopy (AES)/XPS analysis.[21] The elastic-scattering effect diminishes generally the anisotropy of the angular distribution of photoelectrons, leaving a sample as compared to the initial anisotropy. As a result, the inelastic background which is to be removed to obtain the intensity of a signal line becomes a complicated function of the geometry. Figures 6 and 7 clearly indicate that the background may be increased or decreased due to redistribution of electrons over the emission directions. Moreover, the neglect of the elastic-scattering effect may result in the peak intensity being in error up to 20–25 %.

At present, the path-length distribution function cannot be approached experimentally. Verification of the reliability of the proposed models can only be done indirectly by comparing some other characteristics of electron transport obtained experimentally and derived within the same theories. One of them is the angular distribution of photoemission from polycrystalline solids. It was shown that both the analytical and Monte Carlo approaches describe the experimental angular distribution of photoelectrons much better than the straight-line approximation.[12,14] Furthermore, relatively large experimental material on electron elastic backscattering from surfaces is presently available. Several theoretical papers, approaching this problem, were recently published.[13,30–34] Very good agreement was found for angular distributions of elastically backscattered electrons, obtained experimentally, analytically, and by the Monte Carlo technique. Another example has been the theoretical prediction of the presence of double maxima in the energy dependence of the backscattered probability,[33] which was later confirmed experimentally.

It should be noted that the problem of the path-length distribution function is also relevant for elastic peak electron spectroscopy.[35] However, the angular distribution of elastically and quasielastically backscattered electrons depends strongly on the exact shape of the differential elastic-scattering cross section[10,13,31,32] and so does the corresponding path-length distribution function. Therefore no universal dependence of the function $Q(R,\Omega)$ on the ratio R/λ_{tr} is expected in the general case of the elastic reflection problem.

Finally we would like to stress that the results of the present paper are valid only for a homogeneous medium. Finding a depth distribution function for targets of an arbitrary concentration depth profile represents a much more complicated problem. In this case, a helpful approach may be based on the so-called partial escape probability as a function of the depth of origin.[8] The knowledge of the latter quantity allows us not only to obtain the energy spectrum of the signal electrons leaving a specimen but also to reconstruct simultaneously the unknown depth profile.[8]

The formalism presented in this work is of a general physical interest since the concept of the similarity principle can be applied to various boundary problems involving a Boltzmann-type kinetic equation. This refers to neutron and atomic particle transport as well as to radiative transfer.

ACKNOWLEDGMENT

One of the authors (S.T.) acknowledges support from the Danish Natural Science Research Council.

[1]S. Tougaard, Surf. Interf. Anal. **11**, 453 (1988).
[2]S. Tougaard and P. Sigmund, Phys. Rev. B **25**, 4452 (1982).
[3]A. L. Tofterup, Phys. Rev. B **32**, 2808 (1985).
[4]S. Tougaard, Surf. Sci. **216**, 343 (1989).
[5]V. M. Dwyer and J. A. D. Matthew, Surf. Sci. **193**, 549 (1988).
[6]A. L. Tofterup, Surf. Sci. **227**, 157 (1990).
[7]I. S. Tilinin and W. S. M. Werner, Surf. Sci. **290**, 119 (1993).
[8]W. S. M. Werner, I. S. Tilinin, H. Beilschmidt, and M. Hayek, Surf. Interf. Anal. **21**, 537 (1994).
[9]K. M. Case and P. Zweifel, *Linear Transport Theory* (Addison-Wesley, Reading, MA, 1967).
[10]I. S. Tilinin and W. S. M. Werner, Mikrochim. Acta **114/115**, 485 (1994).
[11]I. S. Tilinin and W. S. M. Werner, Phys. Rev. B **46**, 13 739 (1992).
[12]W. S. M. Werner and I. S. Tilinin, Appl. Surf. Sci. **70/71**, 29 (1993).
[13]W. S. M. Werner, I. S. Tilinin, and M. Hayek, Phys. Rev. B **50**, 4819 (1994).
[14]A. Jablonski and J. Zemek, Phys. Rev. B **48**, 4799 (1993).
[15]A. Jablonski and C. J. Powell, Phys. Rev. B **50**, 4739 (1994).
[16]C. S. Fadley, R. J. Baird, W. Siekhaus, T. Novakov, and S. Å. L. Bergström, J. Electron Spectrosc. Relat. Phenom. **4**, 93 (1974).
[17]J. W. Cooper and S. T. Manson, Phys. Rev. **177**, 157 (1969).
[18]H. Ebel, M. F. Ebel, J. Wernisch, and A. Jablonski, Surf. Interf. Anal. **6**, 140 (1984).
[19]A. Jablonski and I. S. Tilinin, J. Electron Spectrosc. Relat. Phenom. (to be published).
[20]S. Chandrasekhar, *Radiative Transfer* (Oxford University Press, London, 1950).
[21]S. Tougaard, Surf. Interf. Anal. **11**, 453 (1988).
[22]L. Landau, J. Phys. (Moscow) **8**, 201 (1944).
[23]S. Tougaard, QUASES Ver.1.2 "Software Package for Quantitative XPS/AES of Surface Nanostructures by Inelastic Peak Shape Analysis."
[24]S. Tougaard, Solid State Commun. **64**, 547 (1987).
[25]S. Doniach and M. Sunjic, J. Phys. C **3**, 285 (1970).
[26]V. V. Sobolev, *Scattering of Light in Atmosphere of Planets* (Nauka, Moscow, 1972) (in Russian).
[27]I. S. Tilinin, Zh. Eksp. Teor. Fiz. **94**, 96 (1988) [Sov. Phys. JETP **67**, 1570 (1988)].
[28]W. S. M. Werner and I. S. Tilinin, Surf. Sci. **268**, L319 (1992).
[29]A. Jablonski and H. Ebel, Surf. Interf. Anal. **11**, 627 (1988).

[30]A. Jablonski, J. Gryko, J. Kraaer, and S. Tougaard, Phys. Rev. B **39**, 61 (1989).
[31]A. Jablonski, Phys. Rev. B **43**, 7546 (1991).
[32]A. Jablonski, H. S. Hansen, C. Jansson, and S. Tougaard, Phys. Rev. B **45**, 3694 (1992).
[33]A. Jablonski, S. Tougaard, and C. Jansson, Phys. Rev. B **47**, 7420 (1993).
[34]L. Zommer, B. Lesiak, and A. Jablonski, Phys. Rev. B **47**, 13 759 (1993).
[35]G. Gergely, Surf. Interf. Anal. **3**, 201 (1981).